Supporting Information

Is (002) the Only One Important? ：An Overall Consideration of Main Exposed Crystallographic Planes on Zn Anode for Getting Dendrite-Free Long-Life Zinc Ion Battery

Yu Wang[a#], Songyao Zhang[b#], Haoqiang Wang[a], Yi Wang[a], Yani Liu,[a] Shuming Dou,[a] Xinrui Miao[b], Wenli Deng[b], Xi Lin[c,], Qunhui Yuan[a,]**

[a]*Shenzhen Key Laboratory of Flexible Printed Electronics Technology, School of Materials Science and Engineering, Harbin Institute of Technology (Shenzhen), Shenzhen 518055, China*

[b] *College of Materials Science and Engineering, South China University of Technology, Guangzhou 510640, China*

[c]*Blockchain Development and Research Institute, School of Materials Science and Engineering, Harbin Institute of Technology (Shenzhen), Shenzhen 518055, China*

[#] *These authors contributed equally to this work.*

* Corresponding author

E-mail address: *yuanqunhui@hit.edu.cn (Q. Yuan)*

Experimental Section

Materials: α-Cyclodextrin (α-CD), Zinc sulfate heptahydrate ($ZnSO_4 \cdot 7H_2O$), Zinc acetate dihydrate ($Zn(CH_3COO)_2 \cdot 2H_2O$), Vanadium (V) oxide ($V_2O_5$) were purchased from Aladdin.

Electrolyte preparation: 2 M $ZnSO_4$ electrolyte was obtained by dissolving $ZnSO_4 \cdot 7H_2O$ in deionized (DI) water. The modified electrolytes ($ZnSO_4$ + α-CD) were prepared by adding different amounts of α-CD (243, 486 and 730 mg, respectively) into 2 M $ZnSO_4$ electrolytes to get clear solutions at concentrations of 5, 10 and 15 mM, respectively.

Synthesis of $Zn_xV_2O_5 \cdot nH_2O$ nanorods cathode: ZVO was synthesized according to a previous research.[1, 2] Briefly, 1.5 mmol V_2O_5 and 1.2 mmol $Zn(CH_3COO)_2 \cdot 2H_2O$ were dissolved into 35 mL DI water, followed by an addition of 5 mL acetone and 2 mL 10% nitric acid. After ultrasonic treatment for 5 min. The mixed solution was transferred into a Teflon-lined stainless-steel autoclave and heated at 180 ℃ for 24 h. After naturally cooled to room temperature, the ZVO was obtained by centrifugation, washed with DI for three times and vacuum dried at 80 ℃ for 12 h.

Material characterization: X-ray diffraction (XRD) profiles of the samples were recorded on a Panalytical Aries with Cu Kα radiation. The morphologies of the samples were revealed by a Crossbeam350 field emission scanning electron microscope (SEM). The plating behaviors of Zn anodes in symmetric cells were observed by an optical microscope (Olympus BX43). Fourier transform infrared spectra (FTIR, Thermo Scientific Nicolet iS50) were recorded in a wavenumber range of 650-4000 cm^{-1}.

Raman spectra (Renishaw Invia) were collected using 532 nm laser. The pH values were determined by Conductivity Meter DDSJ-308F. The contact angles were measured on an Optical Surface Analyzer OSA-100.

Electrochemical measurements: The electrochemical properties of symmetric cells and full cells were tested in CR2032 coin cells, which were assembled in air atmosphere. 2 M $ZnSO_4$ or 2 M $ZnSO_4$ with different concentrations of α-CD aqueous solution was used as the electrolyte. The symmetric cells were composed of two Zn foils (100 μm) separated by a glass fiber separator (Whatman GF/D). For ZVO||Zn full cell, the slurry for cathode material was coated on steel mesh, which was prepared by mixing ZVO, conductive carbon black, and polytetrafluoroethylene (PTFE) binder at a mass ratio of 7:2:1. Galvanostatic charge/discharge cycling tests were carried out on a LAND battery testing system at room temperature. Chronoamperometry (CA) was tested in a symmetric cell. Linear sweep voltametric (LSV) were carried out with a three-electrode setup, where Zn foil was used as the working electrode, and platinum foil and Ag/AgCl electrode were used as counter and reference, respectively. Cyclic voltammetry (CV) were measured on a CHI 760E electrochemical workstation (Chenhua, China).

Zn^{2+} transference number measurement: The Zn^{2+} transference numbers were obtained by alternating-current (AC) impedance and direct-current (DC) potentiostatic polarization measurements using symmetric cells. The cation transference number (t_{Zn}^{2+}) was determined by the following equation,

$$t_{Zn^{2+}} = \frac{I_S(\Delta V - I_0 R_0)}{I_0(\Delta V - I_S R_S)}$$

where ΔV is the voltage polarization applied, I_0 is the initial response current, I_S is the steady-state response current, R_0 and R_S are the electrode interface impedances before and after the polarization, respectively.

Density functional theory (DFT) calculations: *Ab-initial calculations:* The calculations related to the interaction between Zn atom/α-CD molecule and Zn crystal were performed in the Vienna ab initio simulation package (VASP) based on the DFT.[3] The exchange-correlation energy was approximately described by the Perdew-Burke-Ernzerhof (PBE) functional based on the generalized gradient approximation (GGA).[4] The plane wave basis sets with projector-augmented wave (PAW) pseudopotentials were applied.[5] A vacuum layer of 20 Å is applied to each unit cell. For interaction between Zn atom and Zn crystal, the convergence tolerance was set as 1.0×10^{-5} eV for energy, and all the forces on each atom were smaller than 0.01 eV $Å^{-1}$. The plane-wave cutoff energy was set to 300 eV, and the Brillouin zone was sampled by a 2 × 2 × 2 array of k-points in the Monkhorst–Pack grid.[6] The Zn slab was built with two atomic layers in rectangular 3 × 3 supercell with fixing during structural relaxation. For interaction between α-CD molecule and Zn crystal, the convergence tolerance was set as 1.0×10^{-5} eV for energy, and all the forces on each atom were smaller than 0.05 eV $Å^{-1}$. The plane-wave cutoff energy was set to 400 eV, the Brillouin zone sampling was carried out on a Gamma-centered. The Zn slab was built with four atomic layers in rectangular 10 × 10 supercell with fixing during structural relaxation. All the structures discussed in this study were visualized in the Visualization for Electronic and Structural Analysis VESTA).[7]

The adsorption energy (E_a) between Zn slab and Zn atom/α-CD molecule was defined as following equation:

$$E_a = E_{Zn\text{-}slab+Zn/\alpha\text{-}CD} - E_{Zn\text{-}slab} - E_{Zn/\alpha\text{-}CD}$$

where $E_{Zn\text{-}slab+Zn/\alpha\text{-}CD}$ is the energy of the Zn slab bound with Zn atom/α-CD molecule, $E_{Zn\text{-}slab}$ is the energy of the Zn slab, and $E_{Zn/\alpha\text{-}CD}$ is the energy of Zn atom or α-CD molecule.

Quantum chemistry calculations: The calculations of interaction between Zn^{2+}, H_2O and α-CD molecule were performed with Gaussian 09 package.[8] The geometry optimization was performed at B3LYP-D3(BJ)/def2-SVP level.[9-12] Single point calculation after geometry optimization was carried out at B3LYP-D3(BJ)/def2-TZVP. The implicit universal water solvation model based on solute electron density (SMD) was applied in all calculations.[13] The electrostatic potential (ESP) were obtained from Gauss View.

The binding energy (E_b) between Zn^{2+}, H_2O and α-CD molecule

$$E_b = E_{Total} - E_1 - E_2$$

where E_{Total} is the energy of the whole system, E_1 and E_2 are the energies of Zn^{2+}, water molecular or α-CD molecule.

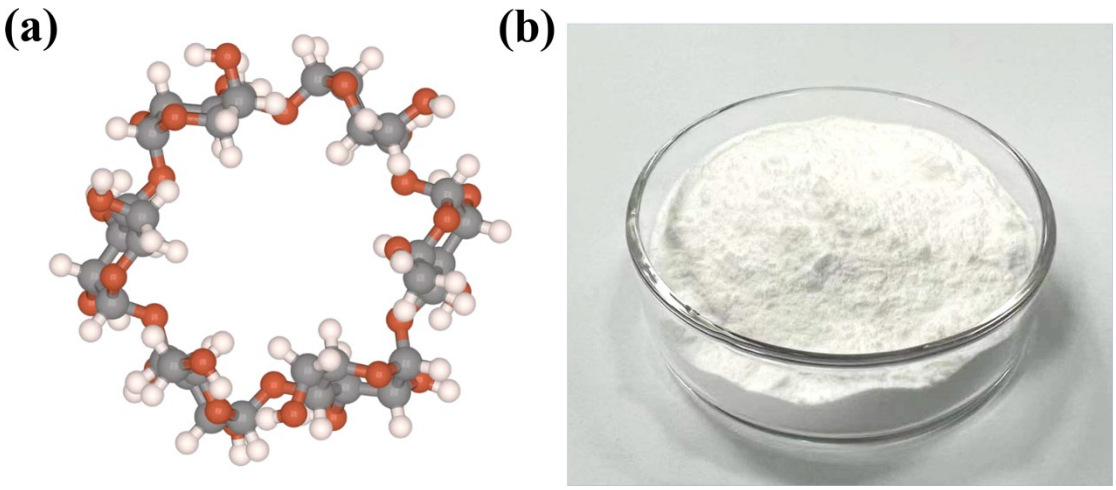

Figure S1. (a) Molecular structure and (b) Optical photo of α-CD ($C_{36}H_{60}O_{30}$).

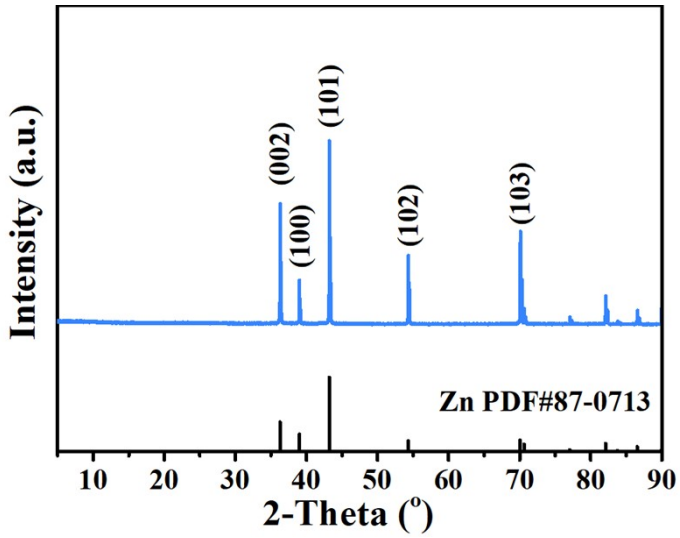

Figure S2. XRD patterns of pristine Zn foil.

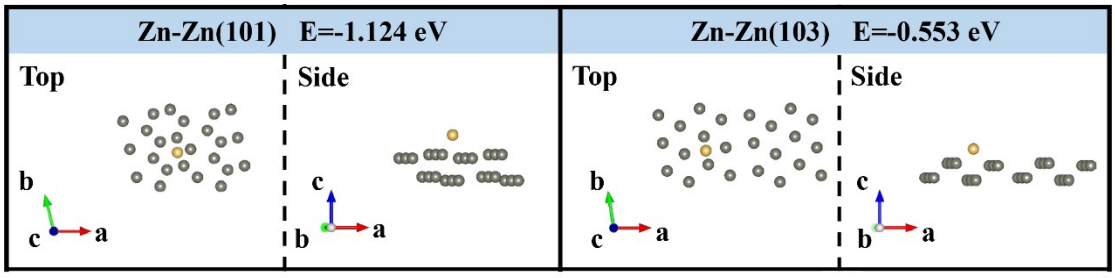

Figure S3. Simulation models of Zn atom adsorbed on the Zn (101) and (103) planes and corresponding adsorption energies.

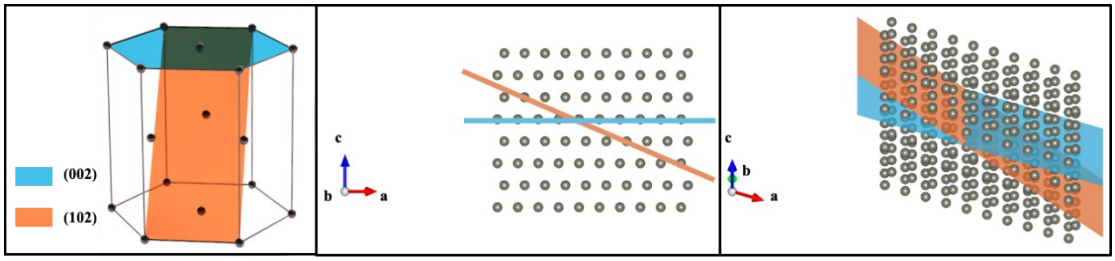

Figure S4. Schematic illustration of the relationship between (102) and (002) planes.

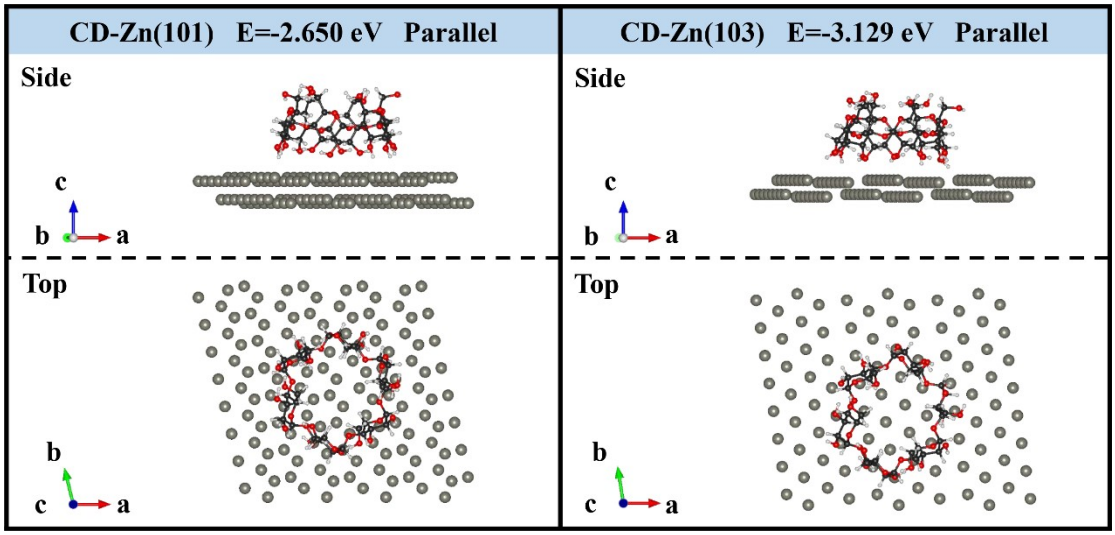

Figure S5. Simulation models of α-CD molecule adsorbed on the Zn (101) and (103) planes and corresponding adsorption energies.

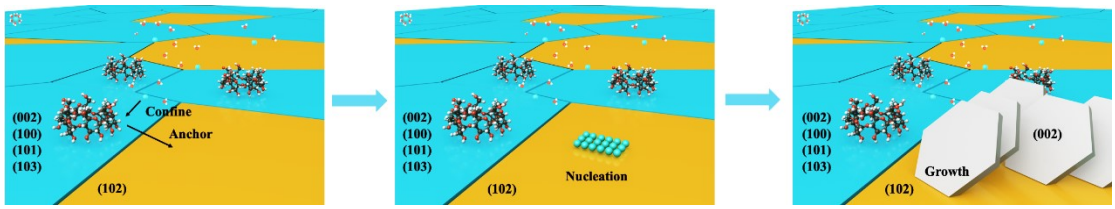

Figure S6. Schematic diagram of the Zn^{2+} plating process in 2 M $ZnSO_4$ + 10 mM α-CD electrolyte.

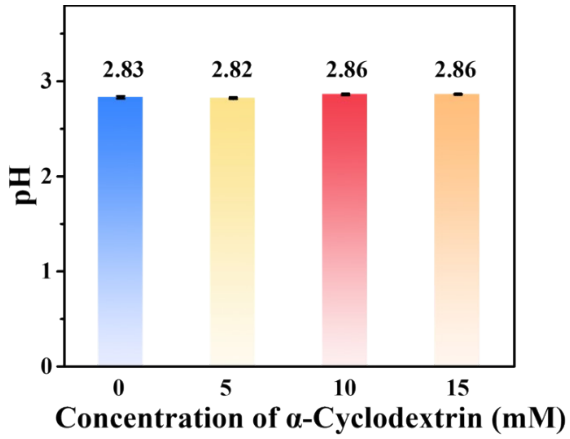

Figure S7. pH values of electrolytes with varied amounts of α-CD additives.

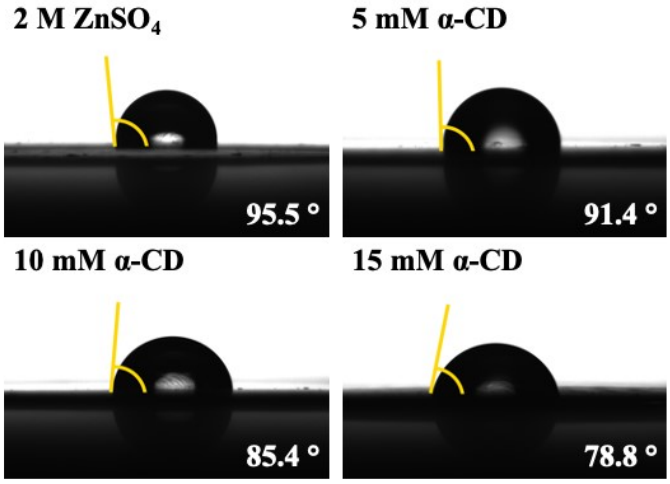

Figure S8. Contact angles of the electrolytes with α-CD additives on Zn foils.

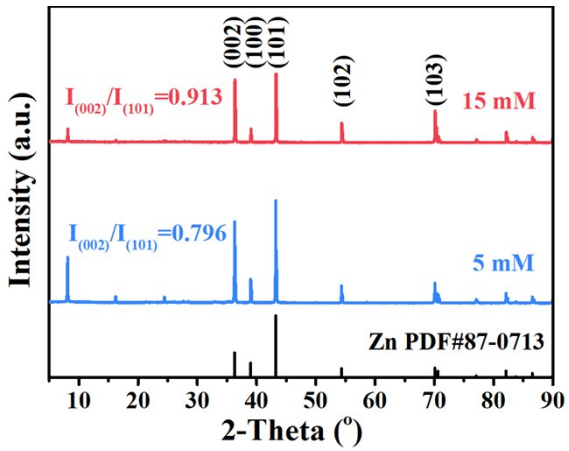

Figure S9. XRD patterns of the Zn anodes cycled for 50 runs in Zn||Zn symmetric cells at a current density of 5 mA cm^{-2} with 5 mA h cm^{-2}, using 2 M $ZnSO_4$ + 5 mM α-CD and 2 M $ZnSO_4$ + 15 mM α-CD, respectively.

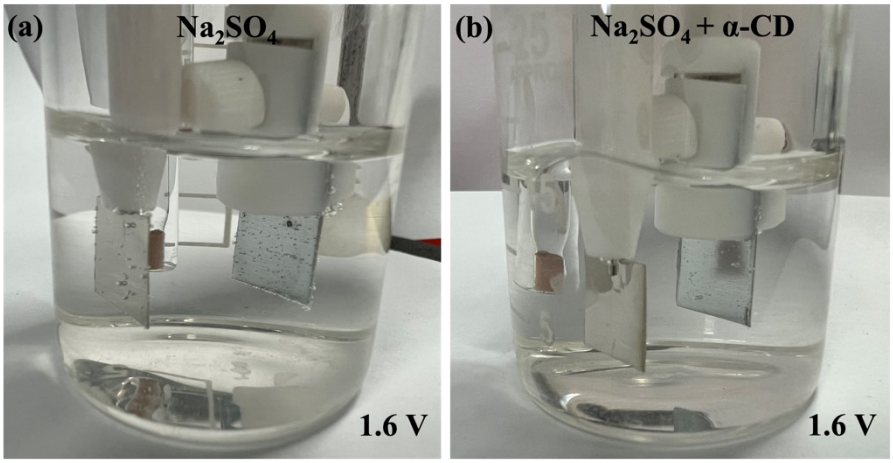

Figure S10. Optical photos showing gas production of cells with modified and unmodified electrolytes at 1.6 V.

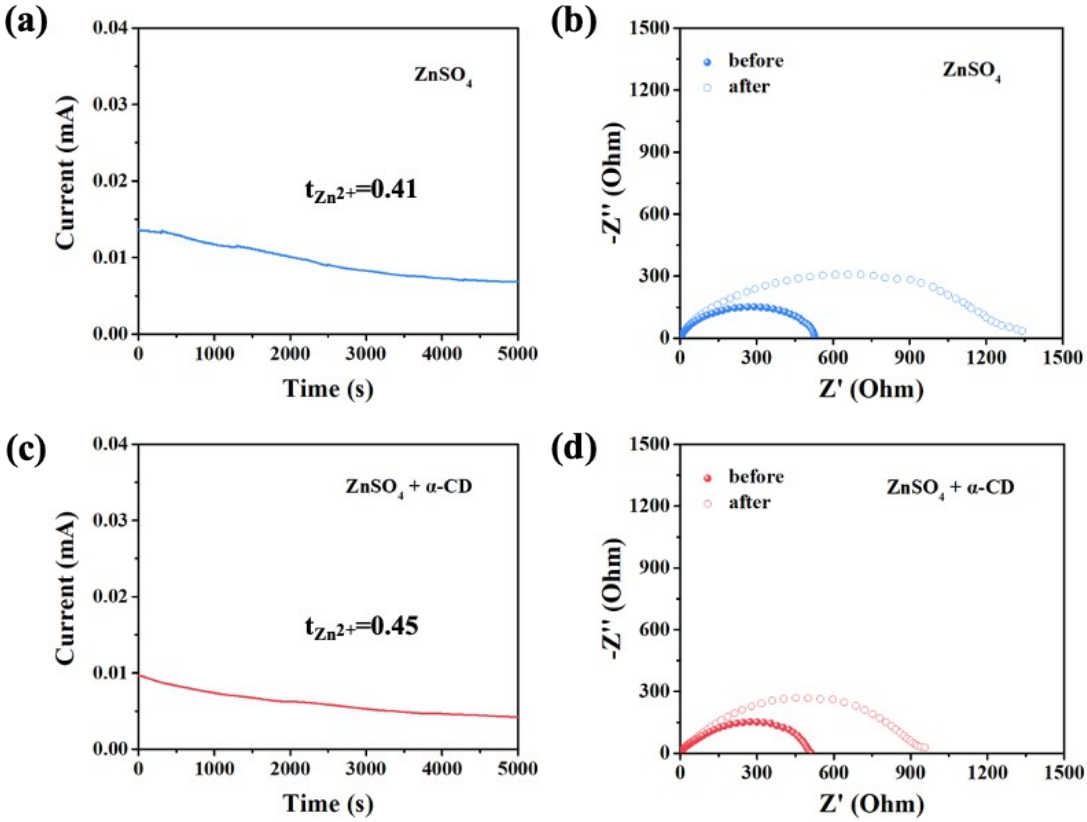

Figure S11. Evaluation on transference number of Zn^{2+} ion. (a, c) Variation of current along time during polarization of Zn||Zn symmetric cell at an overpotential of 10 mV. (b, d) EIS plots of Zn||Zn symmetric cells before and after polarization.

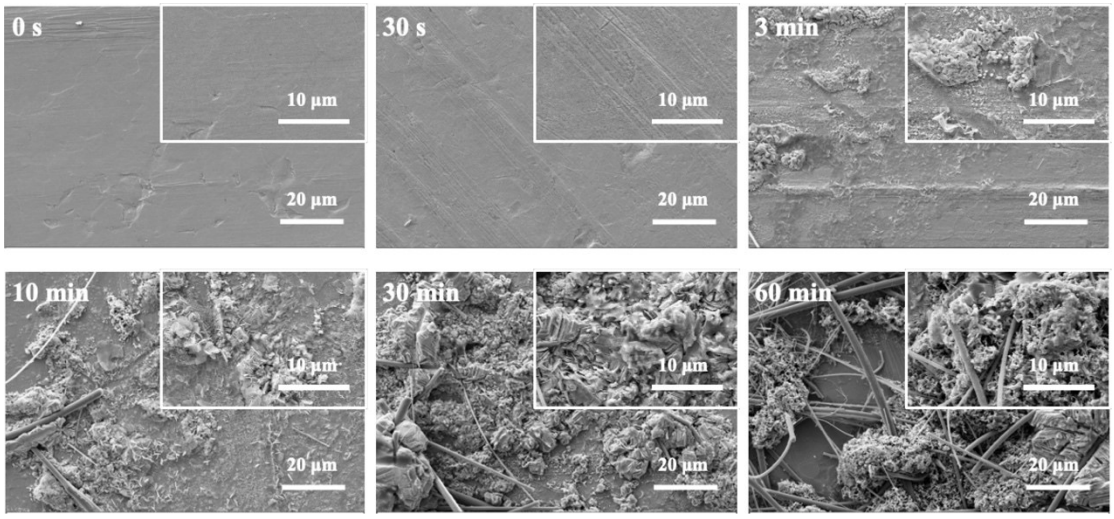

Figure S12. SEM images for morphology evolution of Zn anode in 2 M $ZnSO_4$. Plating current density: 1 mA cm^{-2}.

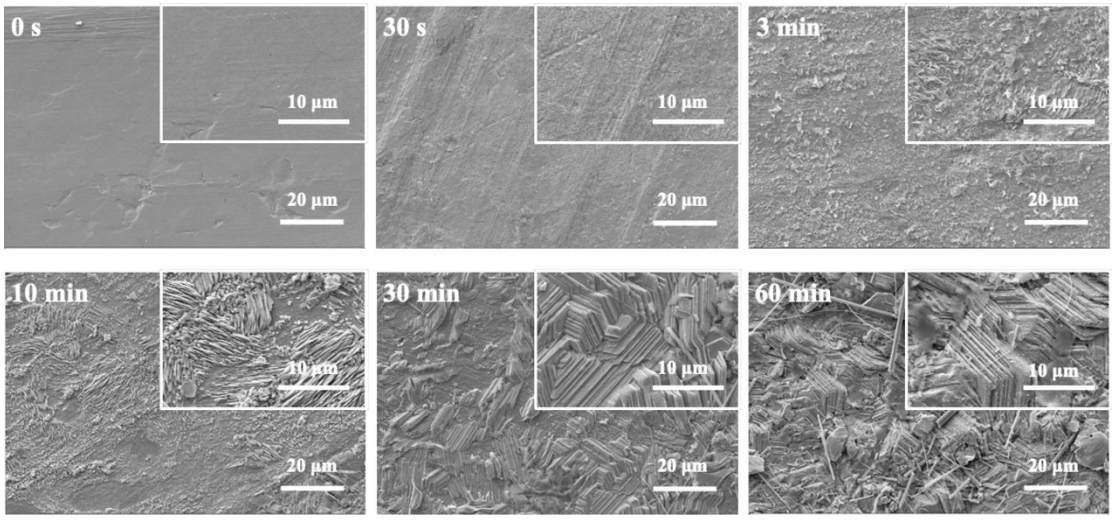

Figure S13. SEM images for morphology evolution of Zn anode in 2 M $ZnSO_4$ + 10 mM α-CD. Plating current density: 1 mA cm^{-2}.

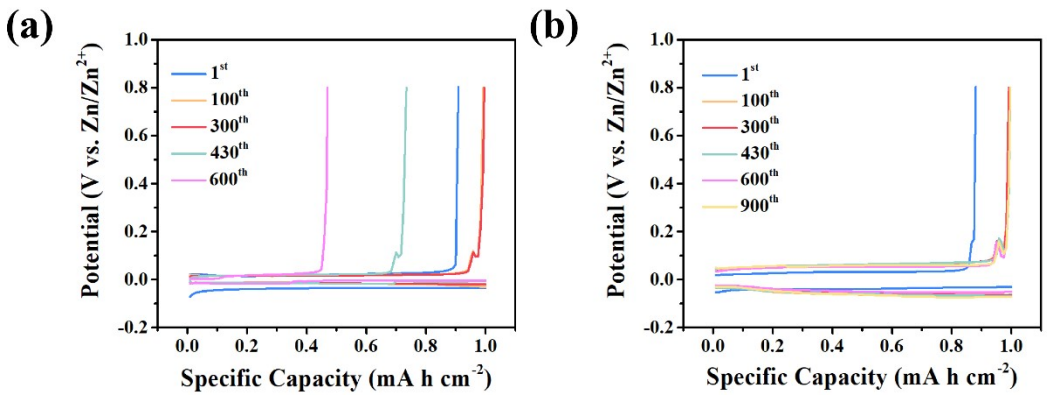

Figure S14. Galvanostatic charge/discharge (GCD) voltage profiles of Cu||Zn cells with (a) 2 M $ZnSO_4$ and (b) 2 M $ZnSO_4$ + 10 mM α-CD.

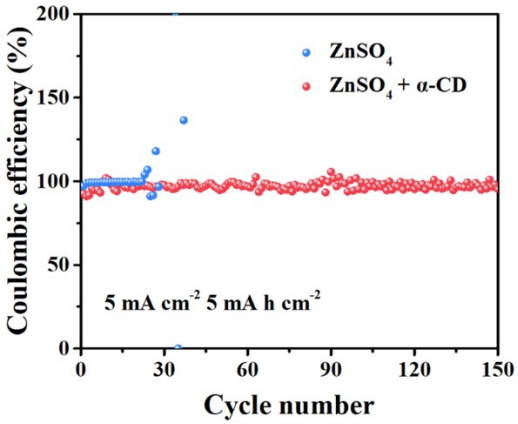

Figure S15. Coulombic efficiency of Cu||Zn asymmetric cells with 2 M $ZnSO_4$ and 2 M $ZnSO_4$ + 10 mM α-CD at 5 mA cm^{-2} with 5 mA h cm^{-2}.

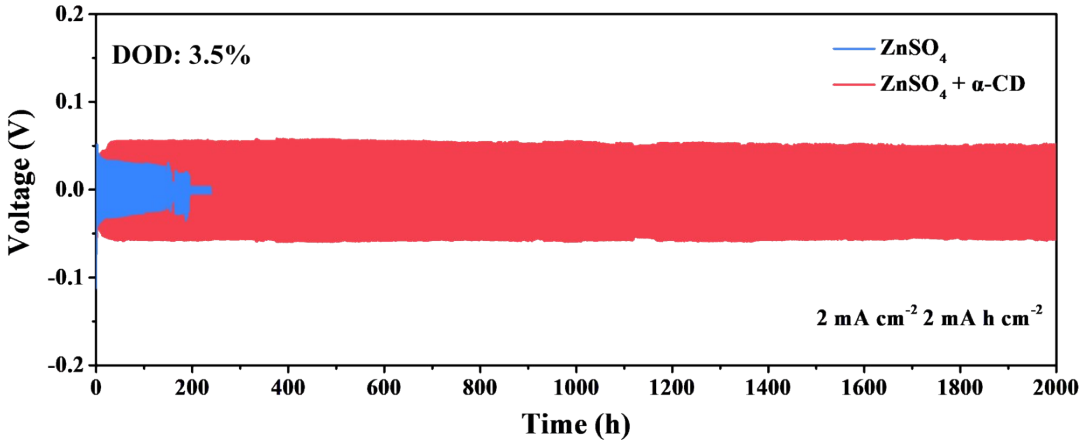

Figure S16. Galvanostatic cycling voltage profiles of symmetric cells with 2 M $ZnSO_4$ and 2 M $ZnSO_4$ + 10 mM α-CD at a current density of 2 mA cm^{-2} with a capacity of 2 mA h cm^{-2}.

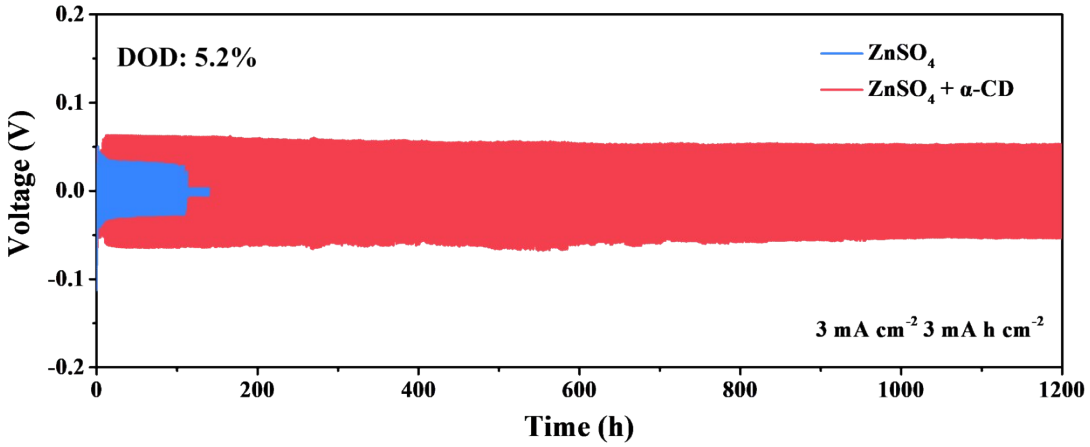

Figure S17. Galvanostatic cycling voltage profiles of symmetric cells with 2 M $ZnSO_4$ and 2 M $ZnSO_4$ + 10 mM α-CD at a current density of 3 mA cm^{-2} with a capacity of 3 mA h cm^{-2}.

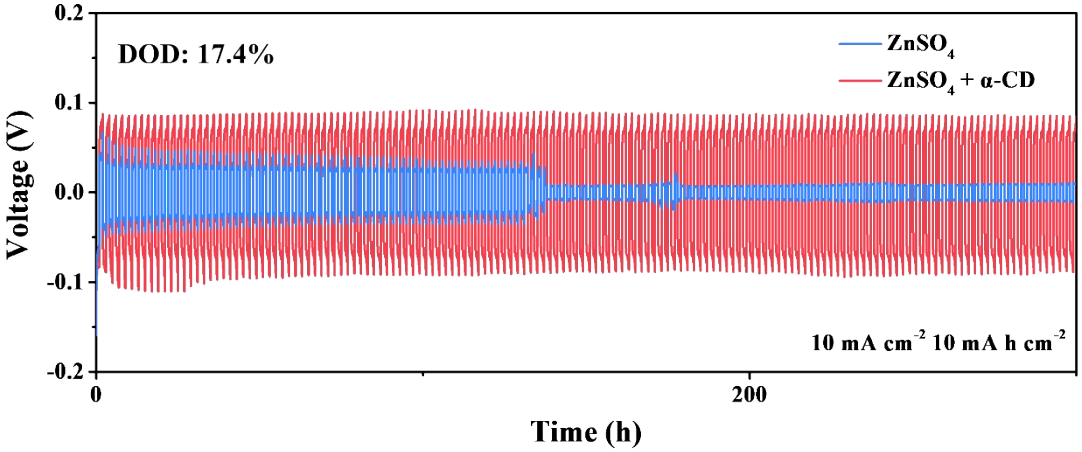

Figure S18. Galvanostatic cycling voltage profiles of symmetric cells with 2 M $ZnSO_4$ and 2 M $ZnSO_4$ + 10 mM α-CD at a current density of 10 mA cm^{-2} with a capacity of 10 mA h cm^{-2}.

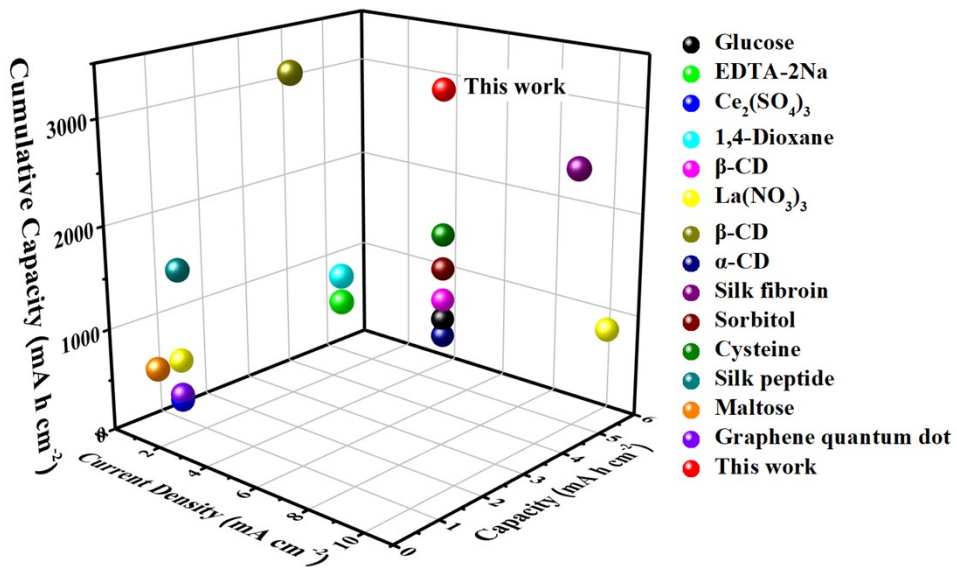

Figure S19. Comparison on the performance of Zn||Zn symmetric cells with different additives from some recently reported works.[14-27]

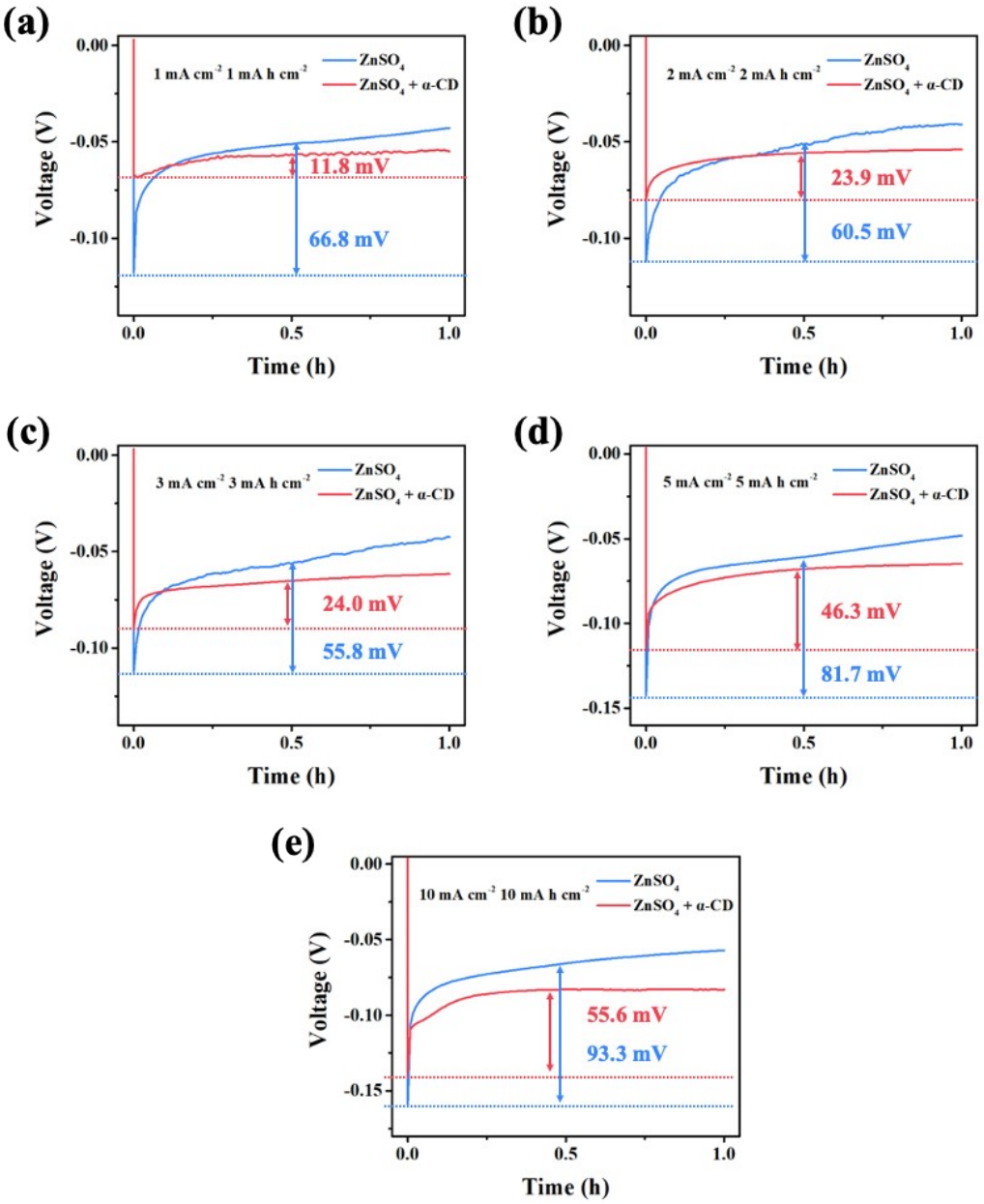

Figure S20. Initial nucleation overpotentials (NOP) at different current densities in 2 M $ZnSO_4$ and 2 M $ZnSO_4$ + 10 mM α-CD. (NOP is taken at 0.5 h.)

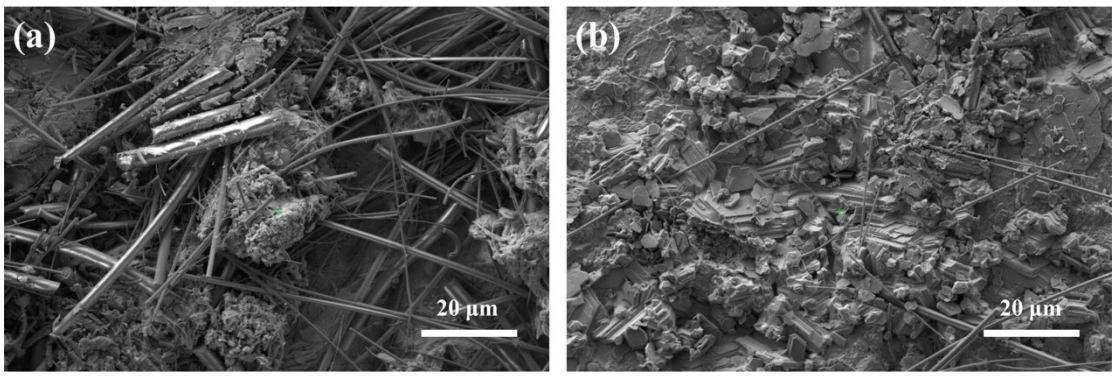

Figure S21. High magnification SEM images of Zn anode in Zn||Zn symmetric cells with (a) 2 M $ZnSO_4$ and (b) 2 M $ZnSO_4$ + 10 mM α-CD after 50 cycles.

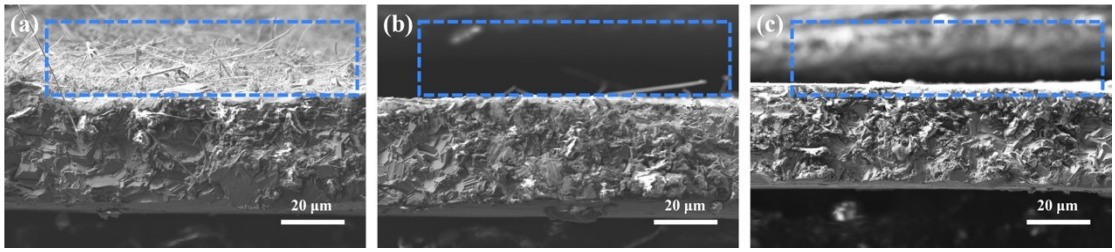

Figure S22. Cross-sectional SEM images of Zn anode in Zn||Zn symmetric cells with (a) 2 M $ZnSO_4$, (b) 2 M $ZnSO_4$ + 10 mM α-CD after 50 cycles, and (c) pristine Zn foil.

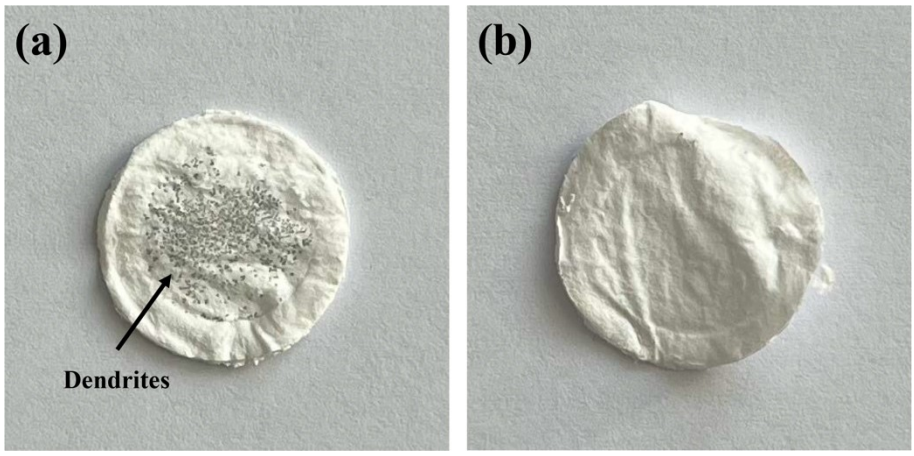

Figure S23. Optical photos of separators obtaining from Zn||Zn symmetric cells with (a) 2 M $ZnSO_4$ and (b) 2 M $ZnSO_4$ + 10 mM α-CD after 50 cycles.

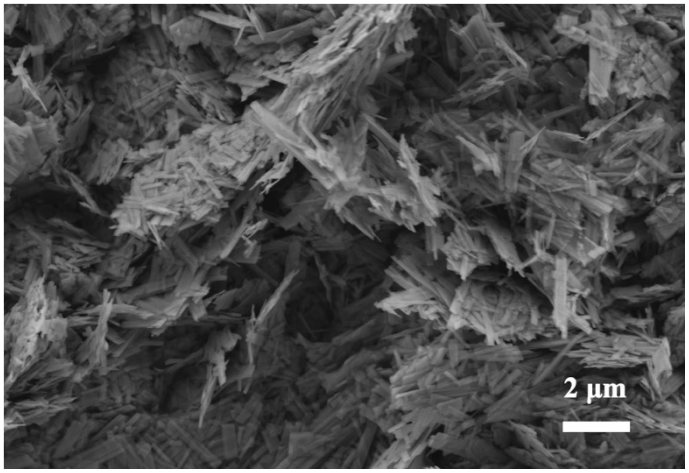

Figure S24. SEM image of ZVO.

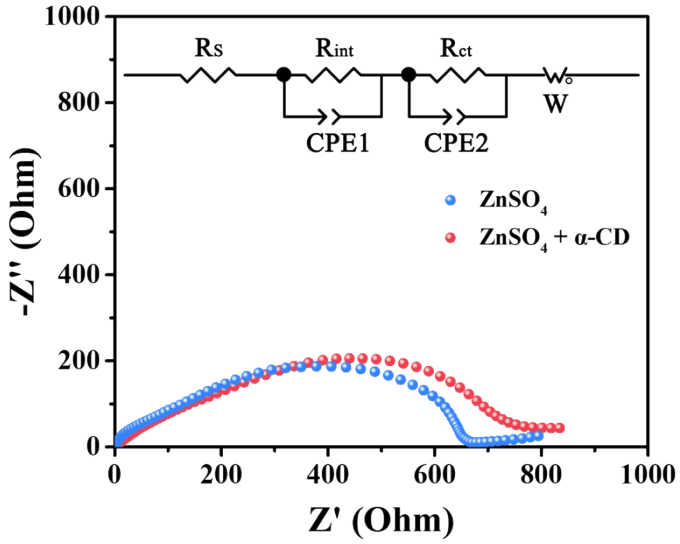

Figure S25. EIS spectra and equivalent circuit diagrams of Zn||ZVO cells using different electrolytes before cycling. R_s, R_{int} and R_{ct} are the electrolyte bulk resistance, interface resistance and charge transfer resistance, respectively.

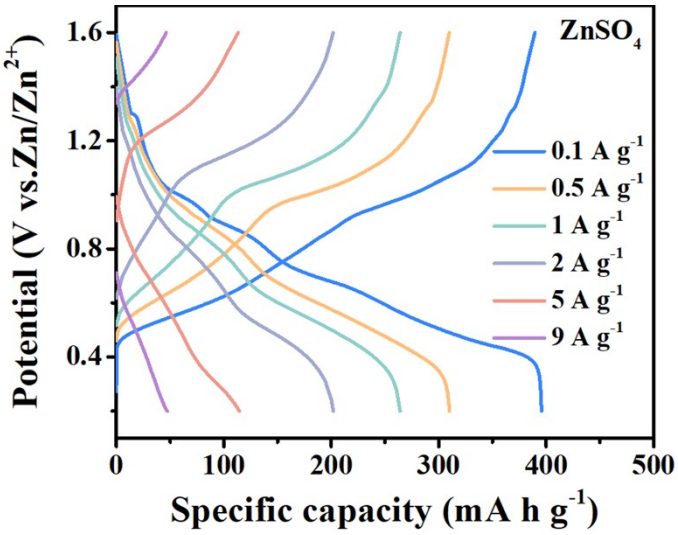

Figure S26. Charge-discharge curves of ZVO||Zn full batteries with 2 M $ZnSO_4$.

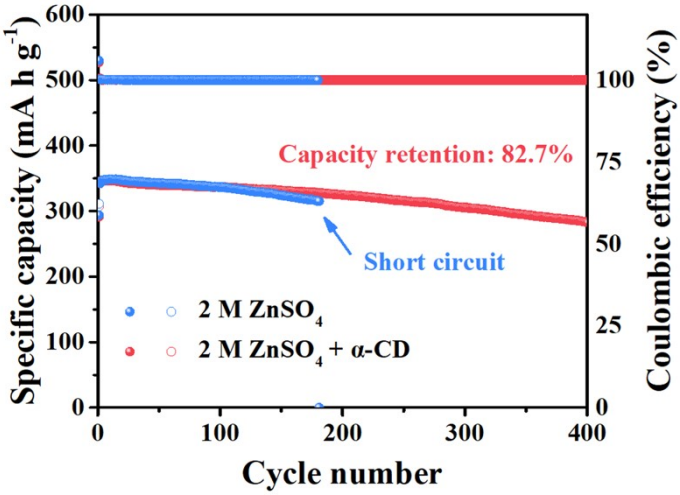

Figure S27. Cycling performance of ZVO||Zn full cell at a current density of 1 A g^{-1} using 50 μm thickness Zn foil.

Table S1. Corresponding corrosion potential and corrosion current density of Linear polarization curves in **Figure 3(b)**.

Samples	Corrosion potential (V vs. Zn/Zn^{2+})	Corrosion current density mA cm^{-2}
2 M $ZnSO_4$	-1.1	1.39
2 M $ZnSO_4$ + 10 mM α-CD	-1.105	0.44

Table S2. Comparison on the performance of Zn||Zn symmetric cells with different additives from some recently reported works.[14-27]

Additive	Electrolyte	Current density (mA cm^{-2})	Capacity (mA h cm^{-2})	Cumulative capacity (mA h cm^{-2})	Depth of discharge/thickness of Zn anode	Reference
Glucose	1 M $ZnSO_4$	5	5	675	100 μm	14
EDTA-2Na	2 M $ZnSO_4$	5	2.5	1250	-	15
$Ce_2(SO_4)_3$	1 M $ZnSO_4$	1	1	200	30 μm	16
1,4-Dioxane	1 M $ZnSO_4$	5	2.5	1500	100 μm	17
β-CD	1 M $Zn(ClO_4)_2$	5	5	875	100 μm	18
$La(NO_3)_3$	2 m $ZnSO_4$	1	1	600	80 μm	19
		10	5.93	160	80%/13 μm	19
β-CD	2 M $ZnSO_4$	4	2	3400	50 μm	20
α-CD	3 M $ZnSO_4$	5	5	500	30%/25μm	21
Silk fibroin	1 M $ZnSO_4$	10	5	2500	150 μm	22
Sorbitol	1 M $ZnSO_4$	5	5	1200	100 μm	23
Cysteine	2 M $ZnSO_4$	5	5	1550	50 μm	24
Silk peptide	2 M $ZnSO_4$	1	1	1500	100 μm	25
Maltose	2 M $ZnSO_4$	1	0.5	600	100 μm	26
Graphene quantum dot	2 M $ZnSO_4$	1	1	250	-	27
α-CD	2 M $ZnSO_4$	5	5	3000	8.7%/100 μm	This work

Table S3. Resistance values deduced from the fitting of EIS curves in **Figure S25**.

Electrolytes	R_s	R_{int}/Ω	R_{ct}/Ω
$ZnSO_4$	0.69	188.40	471.00
2 M $ZnSO_4$ + 10 mM α-CD	0.93	163.30	589.50

References

1. R. Qin, Y. Wang, M. Zhang, Y. Wang, S. Ding, A. Song, H. Yi, L. Yang, Y. Song and Y. Cui, *Nano Energy*, 2021, **80**, 105478.
2. F. Wang, H. Lu, H. Li, J. Li, L. Wang, D. Han, J. Gao, C. Geng, C. Cui and Z. Zhang, *Energy Storage Materials*, 2022, **50**, 641-647.
3. G. Kresse and J. Furthmüller, *Computational materials science*, 1996, **6**, 15-50.
4. J. P. Perdew, K. Burke and M. Ernzerhof, *Physical review letters*, 1996, **77**, 3865.
5. P. E. Blöchl, *Physical review B*, 1994, **50**, 17953.
6. H. J. Monkhorst and J. D. Pack, *Physical review B*, 1976, **13**, 5188.
7. K. Momma and F. Izumi, *Journal of applied crystallography*, 2011, **44**, 1272-1276.
8. M. J. Frisch, G. W. Trucks, H. B. Schlegel, G. E. Scuseria, M. A. Robb, J. R. Cheeseman, G. Scalmani, V. Barone, G. A. Petersson, H. Nakatsuji, X. Li, H. P. Hratchian, A. F. Izmaylov, J. Bloino, G. Zheng, J. L. Sonnenberg, M. Hada, M. Ehara, K. Toyota, R. Fukuda, J. Hasegawa, M. Ishida, T. Nakajima, Y. Honda, O. Kitao, H. Nakai, T. Vreven, J. A. Montgomery Jr., J. E. Peralta, F. Ogliaro, M. J. Bearpark, J. J. Heyd, E. N. Brothers, K. N. Kudin, V. N. Staroverov, R. Kobayashi, J. Normand, K. Raghavachari, A. P. Rendell, J. C. Burant, S. S. Iyengar, J. Tomasi, M. Cossi, N. Rega, J. M. Millam, M. Klene, J. E. Knox, J. B. Cross, V. Bakken, C. Adamo, J. Jaramillo, R. Gomperts, R. E. Stratmann, O. Yazyev, A. J. Austin, R. Cammi, C. Pomelli, J. W. Ochterski, R. L. Martin, K. Morokuma, V. G. Zakrzewski, G. A. Voth, P. Salvador, J. J. Dannenberg, S. Dapprich, A. D. Daniels, O. Farkas, J. B. Foresman, J. V. Ortiz, J. Cioslowski and D. J. Fox, *Journal*, 2009.
9. P. J. Stephens, F. J. Devlin, C. F. Chabalowski and M. J. Frisch, *The Journal of physical chemistry*, 1994, **98**, 11623-11627.
10. S. Grimme, J. Antony, S. Ehrlich and H. Krieg, *The Journal of chemical physics*, 2010, **132**, 154104.
11. S. Grimme, S. Ehrlich and L. Goerigk, *Journal of computational chemistry*, 2011, **32**, 1456-1465.
12. F. Weigend and R. Ahlrichs, *Physical Chemistry Chemical Physics*, 2005, **7**, 3297-3305.

13. A. V. Marenich, C. J. Cramer and D. G. Truhlar, *The Journal of Physical Chemistry B*, 2009, **113**, 6378-6396.
14. P. Sun, L. Ma, W. Zhou, M. Qiu, Z. Wang, D. Chao and W. Mai, *Angewandte Chemie*, 2021, **133**, 18395-18403.
15. J. Cao, D. Zhang, R. Chanajaree, Y. Yue, Z. Zeng, X. Zhang and J. Qin, *Advanced Powder Materials*, 2022, **1**, 100007.
16. Y. Li, P. Wu, W. Zhong, C. Xie, Y. Xie, Q. Zhang, D. Sun, Y. Tang and H. Wang, *Energy & Environmental Science*, 2021, **14**, 5563-5571.
17. R. Feng, X. Chi, Q. Qiu, J. Wu, J. Huang, J. Liu and Y. Liu, *ACS Applied Materials & Interfaces*, 2021, **13**, 40638-40647.
18. M. Qiu, P. Sun, Y. Wang, L. Ma, C. Zhi and W. Mai, *Angewandte Chemie International Edition*, 2022, DOI: 10.1002/anie.202210979.
19. R. Zhao, H. Wang, H. Du, Y. Yang, Z. Gao, L. Qie and Y. Huang, *Nature Communications*, 2022, **13**, 1-9.
20. C. Meng, W. He, L. Jiang, Y. Huang, J. Zhang, H. Liu and J. J. Wang, *Advanced Functional Materials*, 2022, DOI: 10.1002/adfm.202207732, 2207732.
21. K. Zhao, G. Fan, J. Liu, F. Liu, J. Li, X. Zhou, Y. Ni, M. Yu, Y.-M. Zhang and H. Su, *Journal of the American Chemical Society*, 2022, **144**, 11129-11137.
22. J. Xu, W. Lv, W. Yang, Y. Jin, Q. Jin, B. Sun, Z. Zhang, T. Wang, L. Zheng and X. Shi, *ACS nano*, 2022, **16**, 11392-11404.
23. M. Qiu, P. Sun, A. Qin, G. Cui and W. Mai, *Energy Storage Materials*, 2022, **49**, 463-470.
24. Q. Meng, R. Zhao, P. Cao, Q. Bai, J. Tang, G. Liu, X. Zhou and J. Yang, *Chemical Engineering Journal*, 2022, **447**, 137471.
25. B. Wang, R. Zheng, W. Yang, X. Han, C. Hou, Q. Zhang, Y. Li, K. Li and H. Wang, *Advanced Functional Materials*, 2022, 2112693.
26. W. Chen, S. Guo, L. Qin, L. Li, X. Cao, J. Zhou, Z. Luo, G. Fang and S. Liang, *Advanced Functional Materials*, 2022, **32**, 2112609.
27. H. Zhang, R. Guo, S. Li, C. Liu, H. Li, G. Zou, J. Hu, H. Hou and X. Ji, *Nano Energy*, 2022, **92**, 106752.